1   **Measles fusion complexes from central nervous system clinical isolates: decreased**

2   **interaction between hemagglutinin and fusion proteins**

3   Cyrille Mathieu[1,2,3*], Tiago Nascimento Figueira[1,2], Amanda R. Decker[1,2], Marion Ferren[1,2,3],

4   Tiziana F. Bovier[1,2,4], Eric M. Jurgens[1,2,5] , Tara C. Marcink [1,2], Anne Moscona[1,2,6,7], and

5   Matteo Porotto[1,2,4*]

6   [1]Center for Host-Pathogen Interaction, Columbia University Vagelos College of Physicians

7   and Surgeons, New York, New York USA.

8   [2]Department of Pediatrics, Columbia University Vagelos College of Physicians and Surgeons,

9   New York, New York USA.

10   [3]CIRI, Centre International de Recherche en Infectiologie, Team Immunobiology of the Viral

11   infections, Univ Lyon, Inserm, U1111, CNRS, UMR5308, Université Claude Bernard Lyon 1,

12   Ecole Normale Supérieure de Lyon, 69007, Lyon, France.

13   [4]Department of Experimental Medicine , University of Campania, 81100 Caserta , Caserta ,

14   Italy.

15   [5]Weill Cornell Medical College, New York, New York, USA.

16   [6]Department of Microbiology & Immunology, Columbia University Vagelos College of

17   Physicians and Surgeons, New York, New York, USA.

18   [7]Department of Physiology & Cellular Biophysics, Columbia University Vagelos College of

19   Physicians and Surgeons, New York, New York, United States.

20

21   *To whom correspondence should be addressed: Cyrille Mathieu (cyrille.mathieu@inserm.fr)

22   and Matteo Porotto (mp3509@cumc.columbia.edu).

23   **One Sentence Summary:** Measles CNS adapted fusion complexes have altered H/F

24   interaction.

25   **Key words:** Viral fusion; CNS adaptation; viral infectivity.

Abstract:

Measles virus (MeV) viral entry is mediated by a fusion complex comprised of a receptor binding protein (hemagglutinin, H) and a fusion protein (F). The wild type H/F complex requires interaction with specific proteinaceous receptors (CD150/SLAM and nectin-4) in order to be activated. In contrast the H/F complexes isolated from viruses infecting the central nervous system (CNS) do not require a specific receptor. A single amino acid change in the F protein (L454W) was previously identified in two patients with lethal sequelae of MeV CNS infection, and the F bearing this mutation mediates fusion even without the H protein. We show here that viruses bearing the L454W fusion complex are less efficient than wt virus at targeting receptor expressing cells and that this defect is associated with a decreased interaction between the H and the F proteins.

Importance:

Measles (Mev) infection can cause serious complications including measles inclusion body encephalitis (MIBE) and subacute sclerosing panencephalitis (SSPE). MIBE and SSPE are relatively rare but lethal. We have shown that the fusion complex of CNS adapted clinical samples can spread in the absence of known receptor. We now provide evidence that HRC mutations leading to CNS adaptation come at a cost to the efficiency of viral entry.

Introduction:

Despite the availability of an effective measles virus (MeV) vaccine and efforts to increase vaccine coverage by the WHO, UNICEF, and their partners, MeV has not been eradicated and the estimated global measles death toll rose from 89,780 in 2016 to 207,500 in 2019(1). The SARS-CoV-2 pandemic and associated countermeasures reduced the incidence

50   of other respiratory viral infections but also halted vaccination, increasing the risk of measles

51   outbreaks in the future(1).

52   MeV is the most infectious virus known to humans, transmits via the air, and causes systemic

53   infection. The virus enters cells via two cellular receptors: CD150/SLAM expressed by

54   subsets of immune cells(2) and nectin-4 expressed by epithelial cells(3, 4). Central nervous

55   system (CNS) sequelae associated with active viral infection include subacute sclerosing

56   panencephalitis (SSPE) and measles inclusion body encephalitis (MIBE) (5-10). These CNS

57   complications have been associated with viral evolution and specific CNS adaptation,

58   specifically with alterations in the viral fusion mechanism(11, 12).

59   MeV expresses two envelope glycoproteins that make up the fusion complex. The H protein

60   mediates receptor binding, followed by triggering of the F protein, which leads to merger of

61   the viral envelope with target cell membranes. We refer to the H/F pairs of MeV as the viral

62   fusion complex, since these proteins act in concert. F is synthesized as a precursor (F_0) that is

63   cleaved within the cell to yield the pre-fusion F complex comprising three C-terminal F_1

64   subunits associated non-covalently with three N-terminal F_2 subunits. This trimeric F

65   structure is kinetically trapped in a metastable conformation, primed for fusion activation

66   upon engagement of the H glycoprotein by the cell-surface receptor (either CD150/SLAM or

67   nectin-4)(2-4, 13-15). After receptor engagement by H, the pre-fusion F undergoes a structural

68   transition, extending and inserting its hydrophobic "fusion peptide" into the target cell. During

69   entry, F refolds into a so-called "trimer of hairpins" (or 6-helix bundle) post-fusion structure

70   that brings together the N-terminal heptad repeat (HRN) and the C-terminal heptad repeat

71   (HRC), and the viral and cell membranes fuse(16-23). Peptides derived from the HRC region

72   of the F_2 ectodomain inhibit paramyxovirus entry with varying activity(19, 24-32). We and

73   others have shown that fusion complexes from CNS isolated clinical samples are dysregulated

74   and do not require H-receptor interaction for mediating fusion(8, 10, 33, 34), and for a

75   specific mutated F (L454W) even the presence of the H was dispensable for cell-to-cell fusion

76   in transfected cells(8, 10, 34). Here we investigated whether this phenotype was correlated

77   with dimished H-F interaction and we highlight that fusion in the absence of receptor

78   interaction is the combined effect of a decrease in the stability of F as well as a decrease in F's

79   interaction with H.

80   **Results:**

81   ***Measles virus F glycoprotein from neuropathogenic viruses***

82   MeV F glycoproteins with specific single residue alterations (S262R, L454W, T461I,

83   and N462K) have been associated with neuropathogenic measles strains that were either

84   isolated from patients or generated in laboratory settings (9, 12, 34, 35). We mapped these

85   mutations onto x-ray structures of the pre-fusion (36) conformations of F (Fig.1A),

86   highlighting the locations of these mutations in MeV F. The S262R mutation occurs at the

87   interface of three protomers in the head region of the pre-fusion structure. The mutation from

88   Ser to Arg at residue 262 results in a clash within each monomer in the existing crystal

89   structure . These microenvironmental changes are likely to affect the conformational stability

90   of the F. The other three mutations (L454W, T461I, and N462K) were located within the C-

91   terminal heptad repeat domain (HRC). In the pre-fusion structure, the L454W mutation would

92   also perturbs the current pre-fusion structure. The T461I and N462K mutations occur in a

93   well-ordered α-helical region of the HRC domain. These three mutations (L454W, T461I, and

94   N462K) occur in the portion of the HRC domain where the head and stalk regions of the pre-

95   fusion conformation meet. Interactions at this region may be important for stabilizing the pre-

96   fusion state and mutations in this junction would affect stability of the MeV-F prefusion

97   structure, as our previous data have shown (12, 34).

98

99

100   *Impact of hyperfusogenic mutations in F on H-F interaction*

101   We previously suggested that the ability of HRC mutants to fuse in the absence of

102   known receptors could be at least partly due to reduced interaction between H and F(34). The

103   interaction between F and H and the impact of mutations in the HRC domain (*i.e.,* L454W,

104   T461I and N462 may be affected by thermal instability – obscuring the effect of the specific

105   mutations -- we included the highly unstable mutant F-S262R (11, 12, 33, 35) which interacts

106   efficiently with H. H-F interaction was assessed with both the cleavable F proteins (Fig. 2A)

107   and the cleavage site mutant (CSM) version of these F proteins (Fig. 2B), to distinguish

108   between effects on the F_0 and the F_1 form of F. Results are presented as the average of 3

109   separate experiments ± SD (Fig.2C). Densitometric analysis was used to normalize the results

110   to total protein content and to convert the data to graphs (average of 3 separate experiments ±

111   standard deviation; Fig. 2C). There is significant reduction in the amount of F_1 co-

112   immunoprecipitated with H for the HRC hyperfusogenic mutants (*i.e.* , L454W, T461I and

113   N462K) compared to the *wt* F ($P = 0.0023$, $P = 0.0030$ and $P = 0.0014$, respectively; two-way

114   ANOVA with multiple comparisons against *wt* F, corrected with the Dunnett hypothesis test).

115   For the other hyperfusogenic mutant, F S262R, there was more co-immunoprecipitated F_1

116   protein when compared to the HRC mutants. There were no differences in co-

117   immunoprecipitation of F_0. Thus, mutations in HRC associated with a hyperfusogenic

118   phenotype decrease the ability of H to interact with the active F_1 form of F.

119

120   **Viral evolution leads to compensatory mutation**

121   MeV bearing the L454W F protein, when grown at 37^oC in cell culture, acquired a

122   compensatory mutation (E455G) that re-balanced F's stability and dependence on H and

123   cellular receptor for mediating fusion (12). The E455G mutation is shown in Fig. 3A, alone

124   and in combination with L454W. Tryptophan (W454) contains a bulky aromatic sidechain

125   when compared to leucine (L454), while glutamic acid (E455) is larger than glycine (G455).

126   We determined whether the E455G mutation restored H-F interaction (Fig. 3). H-F

127   interaction for wt ,L454W, E455G, and L454W/E455G F proteins is shown in Fig. 3 .

128   Densitometric analysis was used to normalize the results to total protein content and to

129   convert the data to graphs (average of 3 separate experiments ± SD; Fig. 3C). The *wt* versus

130   the L454W F was significantly different (as seen in Fig.2), however the mutant E455G F and

131   the double mutant L454W/E455G F co-immunoprecipitated similarly to the *wt* F. The E455G

132   compensatory mutation in the HRC domain of the F resulted in a *wt* phenotype. We

133   previously showed that E455G restored F's stability (as measured by sensitivity to thermal

134   activation) and restored F's dependence on H-receptor interaction for fusion(12). Fig. 3

135   reveals that E455G also reestablished interaction of H with the active F_1 form of F.

136

137   ***Loss of H-F interaction delays viral entry.***

138   One of the consequences of the loss of interaction between F and H is the loss of

139   protection of F from spontaneous triggering(37). Additionally, hyperfusogenic MeV F HRC

140   mutants proteins are less stable in their pre-fusion state, as measured by their temperature

141   sensitivity, compared to the wt F protein. The hyperfusogenic F proteins mediate fusion even

142   in the absence of either CD150/SLAM or nectin-4 receptors(10, 34). We have shown that this

143   decreased F stability, however, results in viruses that are inactivated at lower temperatures

144   than wt virus (10), because F transitions to its post-fusion state more readily, rendering the

145   viral particle non-infectious. We asked whether the destabilizing mutations in F of the

146   neuropathogenic variants affect viral entry into SLAM-expressing cells (38). To do so, we

147   used an assay developed for a related paramyxovirus, human parainfluenza virus 3 (HPIV3).

148   For HPIV3 we have shown that the kinetics of F protein activation and viral entry modulate

149   the potency of HR derived peptides(37, 39), and therefore this modulation can be used as a

150   tool to quantitate F activation and entry. Applying this strategy to MeV, we determined the

151   sensitivity of MeV F to inhibition by MeV HR derived peptides, using a previously described

152   dimeric HR lipopeptide, HRC4. In Fig. 4A, 1μM of HRC4 peptide was added at time points

153   from 0 to 2 hours during infection of Vero-SLAM cells. Peptide addition at time zero

154   inhibited 100% of infection for all the viruses (wt and the three viruses bearing the mutated F

155   proteins). Peptides added after 1 hour decreased inhibition to 30% for wt virus, meaning that

156   most of the wt virus had already entered, while the mutants bearing F T461I and N462K were

157   50% inhibited and the mutant bearing F L454W was 70% inhibited. After 90 min, the peptide

158   continued to inhibit the mutants (from 20 to 30% of viral entry). No inhibitory effect was

159   observed after 2 hours. This experiment reveals that for wt viruses, the window of HRC4

160   inhibitor sensitivity is significantly shorter than that of the viruses bearing the mutated Fs. The

161   longer time of inhibitor susceptibility of the HRC mutant Fs suggests that wt H-F is more

162   efficient for entry in the presence of receptors.

163

164   ***Easier triggering of HRC hyperfusogenic mutants correlates with longer time to completion***

165   ***of fusion***.

166   For HPIV3, fusion requires engagement of the receptor binding protein (the

167   hemagglutinin neuraminidase, HN) beyond initial triggering of the F protein. This

168   engagement of HN is essential for F's function until membrane merger (37). A similar

169   mechanism of ongoing activation of the fusion process by receptor-engaged H could explain

170   our observations for MeV. We showed that constant interaction with F by receptor-engaged H

171   may allow wt H-F to fuse even in the presence of F-targeted anti-MeV peptides (40). As

172   above, we also previously showed that for HRC peptide fusion inhibitors, adding a lipid

173   moiety improves antiviral potency over time(40). In this case a cholesterol-conjugated dimeric

174   peptide (HRC4) was inhibitory as long as 6h after *in vitro* (41). Without a lipid moiety

175   (HRC1), peptide was effective only at early time points after infection.

176   We hypothesize that the loss of of H-F interaction affects both the triggering of HRC

177   mutants and their ability to fuse in the presence of inhibitor. In Fig. 4B we assessed weak

178   peptide inhibitor (HRC1) for inhibition of wt and mutant F fusion. The assay measures the

179   fusion of cells that express viral envelope glycoproteins (MeV IC323 H/F) with cells that

180   express the MeV receptor SLAM. HRC1 peptide inhibited fusion at early time points (1h, Fig.

181   4 B). As expected, this inhibition decreased below 70% after 3h and below 40% for the wt F

182   and S262R F respectively after 6h. In contrast, for the H/L454W F fusion complex, HRC1

183   peptide inhibited over the time course of this fusion assay, significantly better than for the wt

184   complex (**p value, Mann-Whitney U-Test). A parallel assay was performed with the HRC4

185   peptide, which completely inhibited fusion of all MeV Fs (Fig. S1).

186   HRC peptides are thought to stabilize F protein intermediates during the fusion process

187   after insertion into the target cell membrane but before refolding to the post-fusion state. The

188   stabilization of the transient intermediate state of F by HRC peptides was used to identify

189   discrete steps in the fusion process (37, 42). In Fig. 4C we determined whether the HRC1

190   fusion blockade for the HRC mutated F occurs at the same transitional state. Red blood cells

191   (RBCs) were allowed to interact with cells expressing the MeV F hyperfusogenic mutants

192   along with a chimeric receptor binding protein expressing the MeV H stalk and the globular

193   head of HPIV3 HN. This chimeric protein can engage the sialic acid receptor on the RBCs

194   and initiate MeV F-activation for the neuropathogenic F proteins (8, 34, 43). The read-out for

195   peptide inhibition is irreversible binding of the RBCs to the F-expressing cells and/or fusion.

196   This assay provides a measure of the efficiency with which HRC1 binds and retains F in its

197   transitional intermediate state, preventing membrane merger (Fig.4C). 293T cells co-

198   expressing the chimeric receptor binding protein MeV H-HN and MeV F (hyperfusogenic

199   mutants) were incubated with RBCs at 4 °C, then transferred to 37 °C in the presence of

200   HRC1 peptides (1µM). Zanamivir, a small molecule sialic acid analog that blocks HN-

201   receptor interaction was added after 1 h to disengage cells that were bound by HN-globular

202   head engagement alone. Note that wt F was not used in this assay since it is too stable to be

203   activated under these conditions. The proportion of RBCs either free, reversibly bound by

204   HN-receptor interaction (and therefore released by zanamivir), irreversibly bound by F protein

205   bridging (following insertion of the fusion peptide in the target cell membrane), or fused was

206   quantified. For all three MeV F HRC mutants the larger majority of the cell population

207   remained irreversibly bound and very little fusion was observed, confirming the ability of

208   HRC1 to block F in its transitional state after insertion of the fusion peptide in the target cell

209   membrane. In contrast, the percentage of irreversibly bound cells decreased to 30%

210   concomitantly with an increase in fusion up to 50% for the S262R hyperfusogenic mutant,

211   confirming that this F can "override" inhibition by the peptide. The HRC1 peptide stabilizes

212   the intermediate fusion state for all the F proteins that bear mutations in the heptad repeat

213   domain. Taken together, these results confirm that while the reduction in H-F interaction

214   allows HRC hyperfusogenic mutants to fuse in the absence of receptor — which seems to be a

215   benefit in the CNS— it also decreases their fusion compared to wt virus in presence of

216   receptor by reducing complete fusion after triggering. Outside the CNS, this reduced fusion is

217   a disadvantage.

218

219   **Discussion**

220   The altered HRC region of the CNS-adapted MeV F proteins produced viruses that can fuse

221   and infect without known receptors for H. While H-F interaction is essential for fusion and

222   infection by wt MeV, these F proteins (L454W, T461I and N462K; fig 1A) interact less with

223   H but nevertheless mediate infection *in vitro* (L454W, T461I and N462K) (10, 34), in models

224   of CNS infection (L454W, and T461I)(12) and *in vivo* (L454W) (10) more effectively than

225   wt virus in the absence of SLAM or Nectin-4 receptors. As anticipated based on previous

226   data(10, 12, 34), the hyperfusogenicity conferred by the alterations in the MeV F HRC region

227   affects both functional and physical interactions with H. The E455G revertant restored wt-like

228   properties in the context of the L454W-bearing F , and when introduced singly into the F

229   protein led to an extremely stable F(12) . We speculate that introducing W454 into the

230   prefusion F stalk results in local destabilization that enhances F activation, even in the

231   absence of receptor. The nearby mutation G455 may alter the structure sufficiently to restore

232   the "wt" properties. When the viral quasispecies formed by L454W and L454W/E455G F

233   bearing viruses is cultivated in human brain organoids , the L454W/E455G F bearing virus is

234   eliminated within 10 days confirming that the L454W F bearing virus is fit for growth in CNS

235   tissues(12). The virus bearing the S262R mutation in F is neuropathogenic *in vivo* (11, 35),

236   and we observed no significant differences in H-F interaction. A S262G mutation in F (along

237   with several other mutations) was found in virus from a SSPE clinical case (8). Thus, while

238   destabilizing the F protein significantly improves MeV's ability to spread in the brain, the loss

239   of H-F interaction may not be necessary for CNS adaptation.

240   MeV H-F interaction is key for the steps after F insertion in the target membrane, to

241   complete fusion. The viruses bearing F mutations that lead to CNS spread are more

242   susceptible to fusion inhibitory peptides(10). We attribute this, at least in part, to the fact that

243   the H does not continue to activate F after initial triggering.

244   In Fig. 5 we propose models of viral infection with wt MeV and the CNS adapted

245   variants, incorporating the findings in this work as well as work from others. A common

246   pattern for neuropathogenic F variants is decreased stability of F (as assessed by sensitivitiy to

247   heat) and a fusion complex that mediates cell-to-cell fusion in the absence of either

248   CD150/SLAM or nectin-4(8, 10, 12, 34, 44). These properties confer an infectivity cost, since

249   they are significantly slower to complete the fusion process after inital triggering. These

250   features together with lower viability (10) make these viruses adapt to cell-to cell transmission

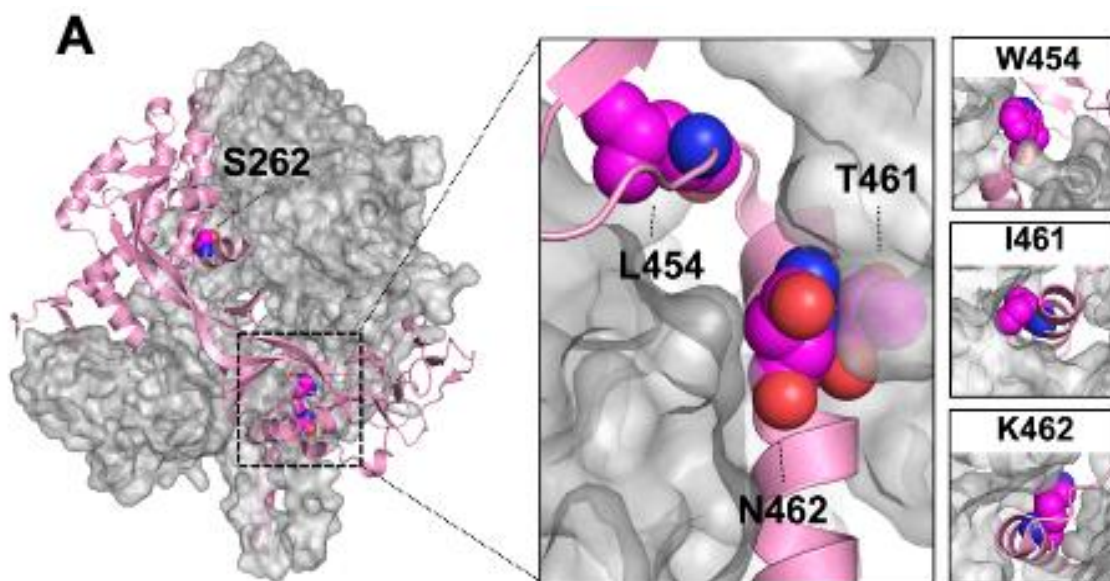251   after initial infection but also likely mean that they are less transmissible.

252

253

256

257 **Figure legends**

258

259 **Figure 1 –** Crystal structure of the trimeric measles F (PDBID:5YXW) in the prefusion state.

260 Monomer is shown in pink. Zoomed in view shows close proximity of residues L454, T461,

261 and N462 near the top of the prefusion F stalk. Left-most panels show potential orientations of

262 mutations W454, I461, and K462 as modeled by pymol with minimal sculpting to reduce
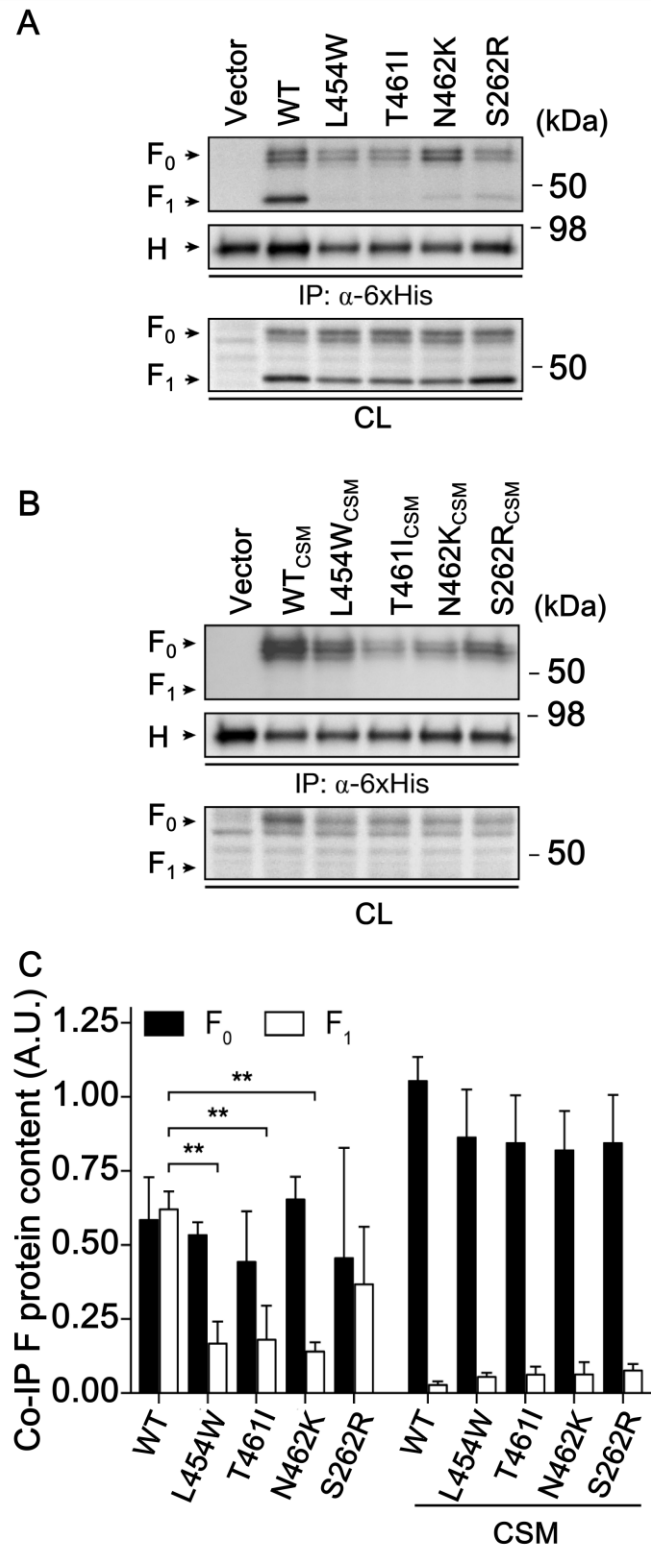
263 steric clashes. Three substitutions (L454W, T461I and N462K) in the HRC domain in

264 neuropathogenic strains are shown. The residue S262 (mutated here to R) was previously

265 described in the hyperfusogenic F variant.

266

267

268

Figure 2 – The effect of hyperfusogenic MeV F HRC domain mutations on MeV H

functional and physical interactions with F_0 and F_1. (A-B) Cell lysates from 293T cell

cultures co-expressing MeV H-6xHis and F *wt*, L454W, T461I, N462K or S262R proteins

were immunoprecipitated with an anti-6xHis antibody. Cleavable (A) and non-cleavable (B)

273   forms of F were included in the experiment. Precipitates were analyzed by western blotting

274   using anti-MeV F HRC and anti-6xHis (top panels) while cell lysates were blotted using anti-

275   MeV F HRC (bottom panels). **(C)** Densitometry measurements of co-immunoprecipitated

276   MeV F protein detected through western blot analysis. Protein content was normalized for the

277   total F protein in cell lysates and the immunoprecipitated H protein. Results are the average of

278   three independent replicates. Error bars correspond to the standard deviation. **, $P \leq 0.01$.

279

280

281
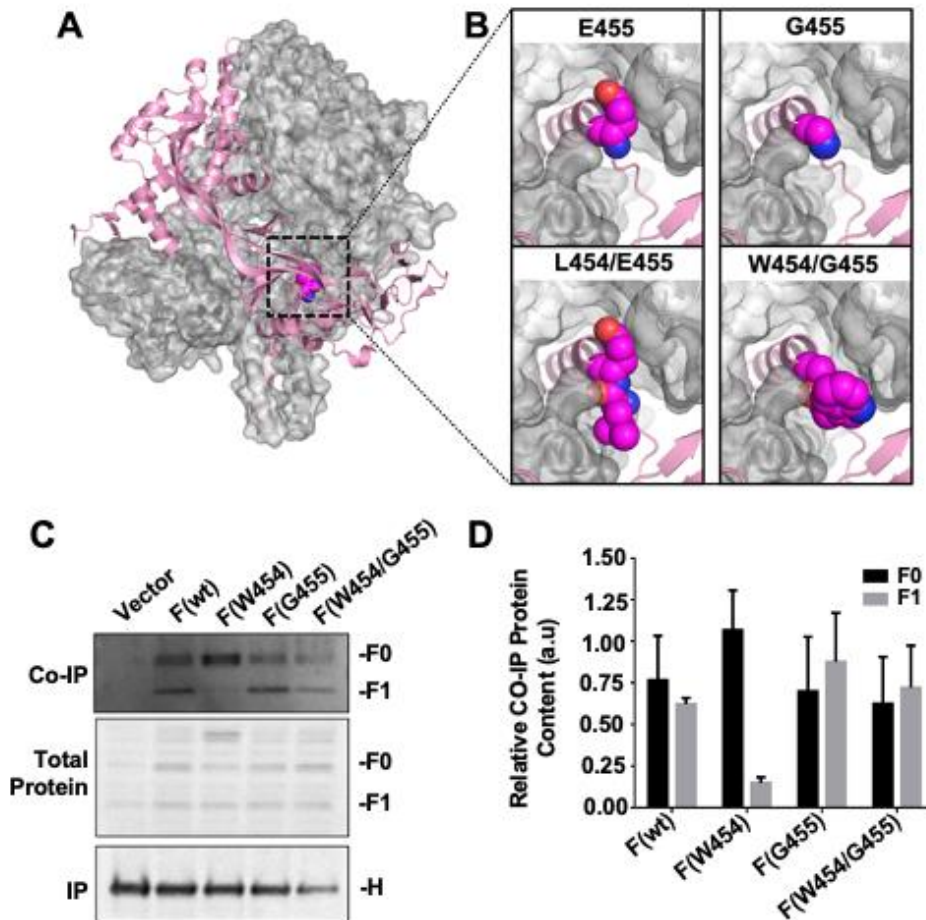
Figure 3 – The effect of F protein's E455G compensatory mutation on H protein's interaction with F_0 and F_1.(A) Prefusion F crystal structure (PDBID: 5YXW). (B) Zoomed in views near the top of the prefusion F stalk region with E455 (top left) and L454/E455 (bottom left) shown as spheres. Mutations G455 (top right) and W454/G455 (bottom right) were substituted in pymol with minimal sculpting to reduce steric clashes. **(C and D)** Cell lysates from 293T cell cultures co-expressing MeV H-6xHis and F *wt*, L454W, E455G, or L454W/E455G proteins were immunoprecipitated with an anti-6xHis antibody. Cleavable (B) and non-cleavable (C) forms of F were included in the experiment. Precipitates were analyzed through western blotting using anti-MeV F HRC and anti-6xHis (top panels) while cell lysates were blotted using anti-MeV F HRC (bottom panels). **(D)** Densitometry measurements of co-immunoprecipitated MeV F protein detected by western blot analysis. Protein content was

293   normalized for the total F protein in cell lysates and the immunoprecipitated H protein. There

294   was no statistical difference (unpaired T-test) between the levels of F_0 that were co-

295   immunoprecipitated for each allele. There was also no statistical difference between F(*w*t) and

296   either allele that contained E455G (single and double mutant) for F_1 levels. However, the

297   difference between the F(*wt*) and F(L454W) F_1 that co-immunoprecipitated with H was

298   extremely statistically significant (P = 0.0007). Error equals +/- SEM. N = 3 biological

299   replicates

300

301
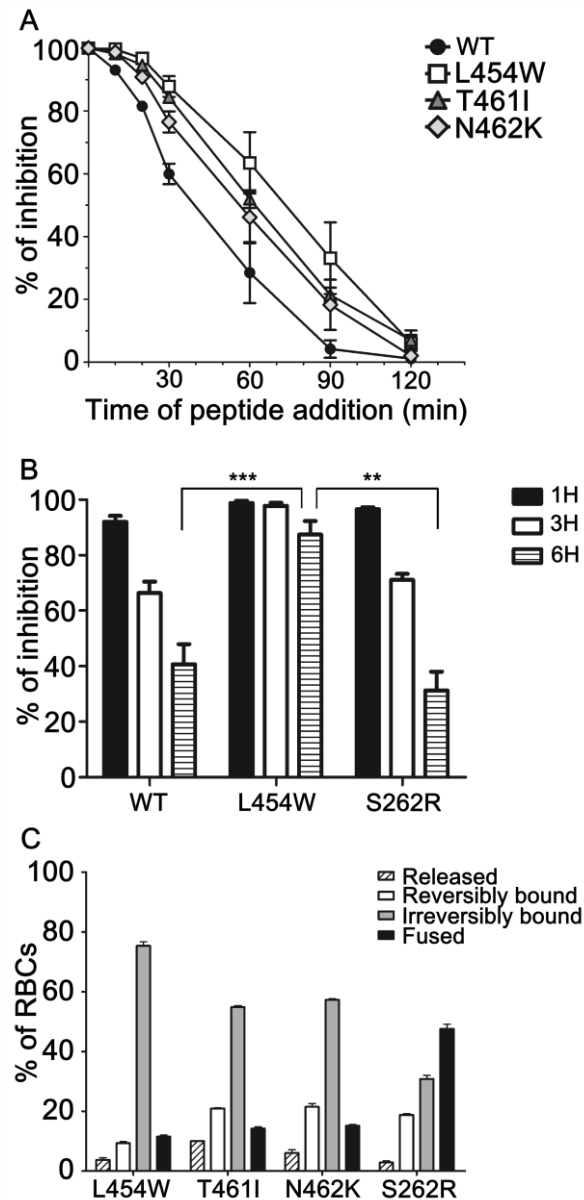
Figure 4 – HRC hyperfusogenic mutants fuse less in presence of entry receptor- (**A**) Inhibition by MeV HRC4 peptides added at different times after infection reveals differences in the rate of F activation. Vero-SLAM cells were infected with wt or the indicated viruses at a multiplicity of infection of 6.7×10^{-4}. The MeV HRC4 fusion inhibitory peptide was added at the time points noted to a final concentration of 1 µM. Cells were overlaid with agarose at 90 min and plaques were stained and counted at 36 h. The percent inhibition of viral entry, normalized to 100% inhibition at time zero, is shown as a function of the time of peptide addition. Data points are means (± standard error) for triplicate experiments. **-** (**B**) Fusion of MeV H/F co-expressing cells with SLAM-bearing cells in the presence of unconjugated

312   peptides (HRC1 at 1 μM) was quantitated at 1 h , 3h or 6 h using a β-galactosidase

313   complementation assay. Results are presented as percent reduction in luminescence (*y* axis)

314   compared with no treatment. Each point is the mean (± standard error) of results from 3 to 5

315   separate experiments (**, $P < 0.01$; ***, $P < 0.001$ [Mann-Whitney-U test]). (**C**) Role of

316   receptor binding protein (H-HN) after F has inserted its hydrophobic fusion peptide into the

317   target cell: progression to membrane merger in the presence of H-F interaction. If H-F

318   interaction is functional, processed F is activated to the stage of fusion peptide insertion

319   captured by unconjugated peptides, and then proceeds to membrane merger. Monolayers of

320   cells co-expressing H-HN and processed F proteins (as indicated on the axis) were allowed to

321   bind to receptor-bearing RBCs at 4°C. Unbound RBCs were washed away, and cells were

322   incubated with standard HRC1 peptides (1 μM) at 37°C for 60 min. The values on the *y* axis

323   reflect the quantity of RBCs that were released by H-HN neuraminidase (striped bar),

324   reversibly bound by H-HN-receptor interaction (white bar), irreversibly bound (gray bar), or

325   fused (black bar). The values are means (±standard deviations) of results from triplicate

326   samples and are representative of the experiment repeated at least four times.
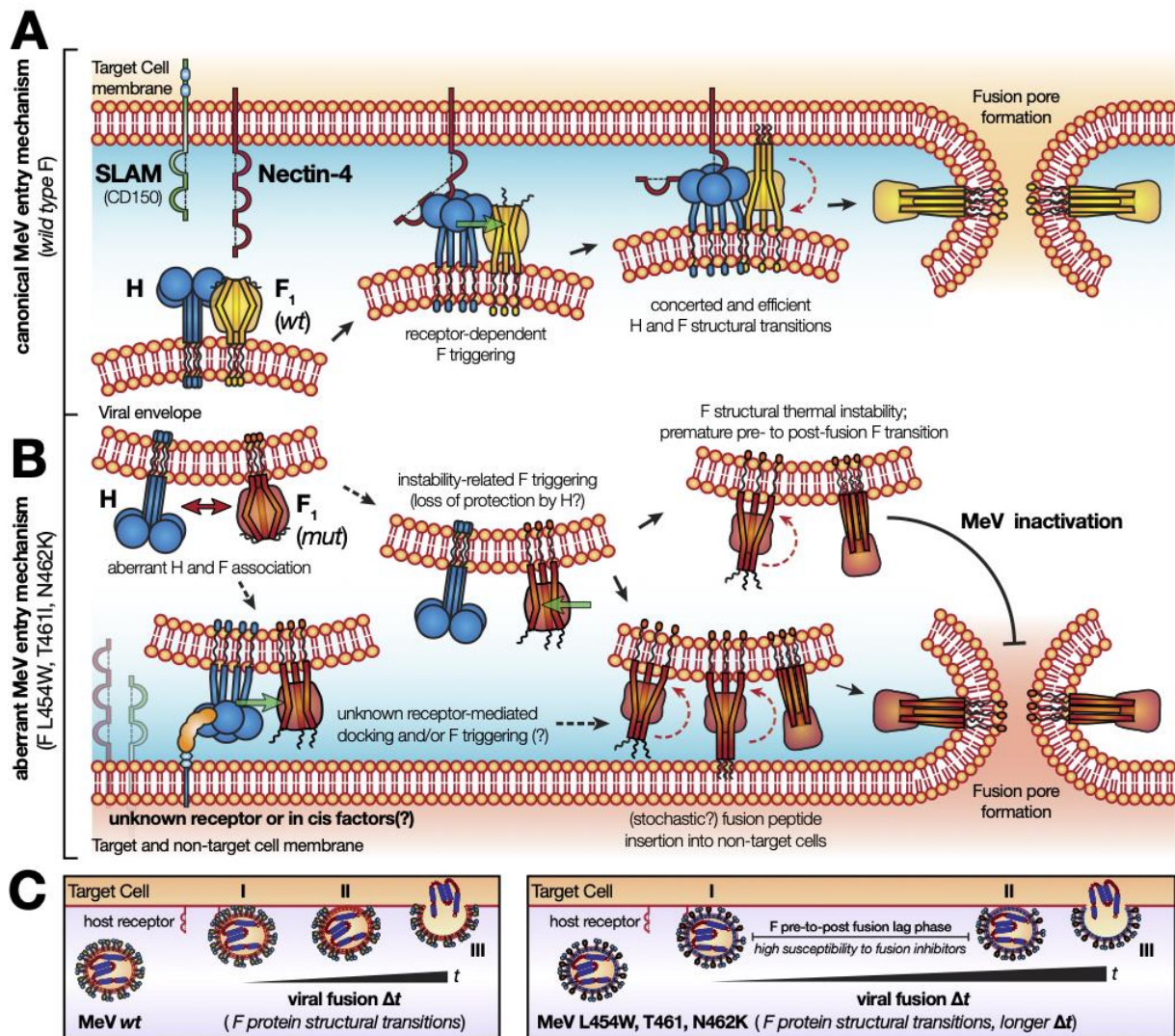
Figure 5 – Model for the hyperfusogenic entry mechanism of neuropathogenic MeV mutant strains. (**A**) The *wt* MeV entry mechanism is characterized by the concerted action of the H and F glycoprotein complex. Upon H-mediated CD150/SLAM or Nectin-4 receptor recognition, and subsequent F triggering, both H and F undergo a series of conformational changes that guide fusion of the cell membrane and viral envelope. H anchors the virus to the cell surface and activates the F to insert its fusion peptide trimers into the cell membrane and undergo a conformational transition, the driving force for lipid mixing and fusion. (**B**) The hyperfusogenic phenotype of neuropathogenic MeV variants is associated with single amino acid mutations in F (L454W, T461I and N462K). Altered association with H triggers the mutated F into unstable fusogenic conformations. The lower energy barrier between the pre-

338   and post-fusion (6HB) conformations leads to premature structural transitions of F and

339   consequent viral attenuation/inactivation. Yet, the mutated F can insert into non-targeted cell

340   types, such as neurons, promoting MeV aberrant infection. **(C)** The coordinated structural

341   transitions of H and F promote entry by *wt* MeV after receptor engagement (left panel). In

342   hyperfusogenic MeV variants, with loss of H-to-F interaction, entry kinetics are slower, with a

343   lag between the F pre- and post-fusion conformations (right panel). This feature enhances

344   susceptibility to F-specific fusion inhibitory peptides acting at this stage.
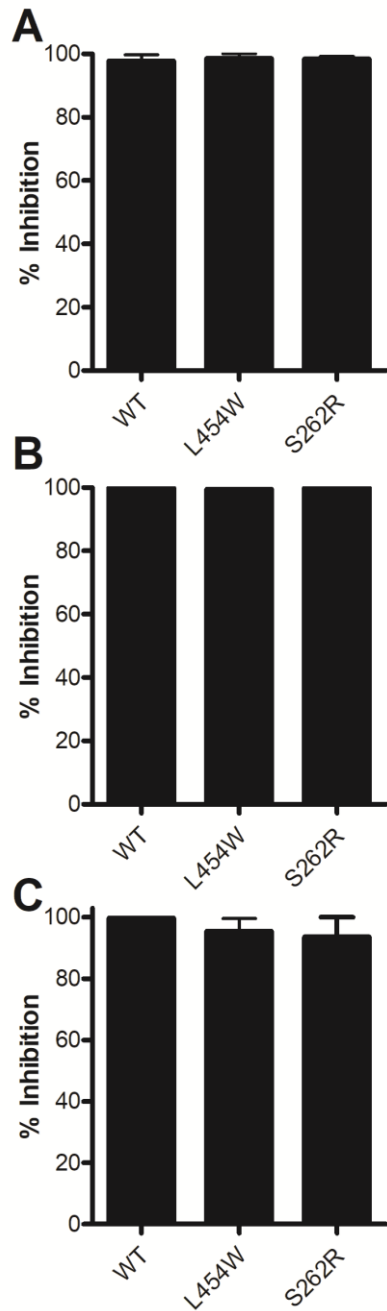
FIG S1. Fusion of MeV H/F co-expressing cells with SLAM-bearing cells in the presence of unconjugated peptides (HRC4, dimer peptide with cholesterol, 1 μM) was quantitated at 1 h (**A**) 3h (**B**) or 6 h (**C**), using a β-galactosidase complementation assay. Results are presented as percent reduction in luminescence (*y* axis) compared with no treatment. Each point is the mean (± standard error) of results from 3 to 5 experiments.

352   **Materials and Methods**

353   ***Peptides:*** MeV F derived fusion inhibitor peptides HRC1 and HRC4 were previously

354   described (40). Briefly 36aa long peptides derived from the heptad repeat region at the C-

355   terminal of the MeV F protein were synthesized (using the wt sequence or the L454W

356   sequence). Monomeric unconjugated (HRC1) or dimeric cholesterol conjugated (HRC4)

357   forms of the peptides were used in this study.

358   ***Plasmids and reagent.*** The genes of MeV IC323 H and F proteins were codon optimized,

359   synthesized, and sub cloned into the mammalian expression vector pCAGGS. Plasmids

360   encoding nectin 4 and CD150/SLAM were commercially acquired.

361   ***Cells.*** 293T (human kidney epithelial) and Vero-SLAM (African green monkey kidney) cells

362   were grown in Dulbecco's modified Eagle's medium (DMEM; Gibco, Invitrogen)

363   supplemented with 10% fetal bovine serum (FBS) and antibiotics in 5% CO_2. The Vero-

364   SLAM culture medium was supplemented with Geneticin.

365   ***HRC4 Peptide time addition related inhibition***. Dulbecco's Modified Eagle's medium

366   (DMEM) containing the indicated viruses (MeV IC323-EGFP, MeV IC323-EGFP-F L454W,

367   MeV IC323-EGFP-F T461I, MeV IC323-EGFP-F N462K all these viruses are from(34)) was

368   used to infect sub-confluent VERO-SLAM cells in 6 well plates (100pfu/well) for 2h at 32°C.

369   MeV HRC4 dimeric fusion inhibitory peptide (1µM) was added to the medium at time points

370   from 15 to 120 min after the beginning of infection. After 2h of incubation with the virus,

371   medium was replaced with medium containing Avicel. Viral titers were assessed after 3 days

372   of incubation at 32°C by immune staining.

373   ***Beta-Galactosidase (Beta-gal) complementation-based fusion assay.*** The beta-gal

374   complementation-based fusion assay was performed as described previously(34). Briefly,

375   293T cells transiently transfected with the constructs indicated above and the omega reporter

376   subunit were incubated for the indicated period with cells coexpressing viral glycoproteins

377   and the alpha reporter subunit in presence or not of MeV F HRC derived peptide (40).

378   ***RBC fusion assay.*** RBC fusion assays were performed on HEK 293T cells transiently

379   expressing MV H_Y17H HPIV3_T193A chimerae (43) and the indicated MeV Fs. Cell

380   monolayers were washed three times with serum-free medium, placed at 4°C with 1% RBC in

381   DMEM for 30 min, then treated with the indicated peptide and placed at 37°C. Zanamivir was

382   added at a final concentration of 10 mM and the cells were incubated at 4°C, rocked, and the

383   liquid phase was collected in V-bottomed 96-well plates for measurement of reversibly bound

384   RBCs. The cells were then incubated at 4°C with ACK-Lysing buffer, and the liquid phase

385   was collected in V-bottomed 96-well plates for measurement of irreversibly bound RBCs. The

386   cells were then lysed in lysis buffer and transferred to flat-bottom 96 well plates for

387   quantification of fused RBCs. The amount of RBCs in each of the four compartments

388   (released, reversibly bound, irreversibly bound, and fused) was determined by measurement

389   of absorption at 410 nm.

390   ***Co-Immunoprecipitation.*** 293T cells were seeded in biocoated 6-well plates (Corning) at

391   5×10^5 cells/well and incubated for 24h, at 37° C. Cells were transfected with plasmid vectors

392   encoding for MeV H-6xHis, MeV F (*wt*, L454W, T461I, N462K ,E455G, L454W/E455G and

393   S262R) and mCherry (6:4:1 mixtures; 2.2 μg/well) using Lipofectamine® 2000 (Invitrogen),

394   according to the manufacturer's recommendations. Transfected cultures were grown at 32° C,

395   overnight, in the presence of HRC1 peptide (1 μM), to minimize cell-cell fusion. mCherry

396   fluorescence was used to monitor cell transfection efficiency after 18h. Prior to cell lysis, cell

397   protein expression was synchronized with cycloheximide (Sigma, 0.1 mg/mL), followed by

398   membrane protein cross-linking with 3,3'-dithiobis(sulfosuccinimidyl propionate) (Sigma; 1

399   mM), at low temperature. The cross-linking reaction was quenched with 20 mM Tris, 150

400   mM NaCl, pH 7.5. Cells were lysed with 50 mM HEPES, 100 mM NaCl, 0.05 g/mL dodecyl

401   maltoside, pH 7.5, supplemented with complete protease inhibitor cocktail (Roche). Lysates

402   were centrifuged at 16000 g for 10 min to remove nuclei and cell debris, and the supernatant

403   was collected for immunoprecipitation and total protein content analysis. MeV H-6xHis

404   protein was immunoprecipitated from cell lysates using Dynabeads® (Thermo, 1 mg/mL)

405   coated with a 6xHis tag-specific antibody (mouse monoclonal, Thermo, MA1-21315).

406   **For Fig.2:** Co-immunoprecipitated and cell lysate proteins were analyzed by western blotting,

407   using primary antibodies specific for MeV F HRC (rabbit polyclonal, Genscript, 503028-1)

408   and 6xHis tag (rabbit polyclonal, Thermo, PA1-983B), followed by an HRP-conjugated anti-

409   rabbit secondary antibody (Kindle Biosceiences, R1006). Western blots were developed using

410   the SuperSignal West Femto substrate (Thermo) and imaged on a *Kwik*Quant^{TM} Imager UV

411   (Kindle Biosciences).

412   **For Fig. 3:** Co-immunoprecipitated and cell lysate proteins were analyzed by western

413   blotting, using primary antibodies specific for MeV F HRC (rabbit polyclonal, Genscript,

414   503028-1) and 6xHis tag (rabbit polyclonal, Thermo, PA1-983B), followed by

415   WesternBreeze Chromogenic Immunodetection Protocol for detection.

416

417   **Literature cited**

418   1.   Durrheim DN, Andrus JK, Tabassum S, Bashour H, Githanga D, Pfaff G. 2021. A
419   dangerous measles future looms beyond the COVID-19 pandemic. Nat Med 27:360-
420   361.
421   2.   Tatsuo H, Ono N, Tanaka K, Yanagi Y. 2000. SLAM (CDw150) is a cellular receptor
422   for measles virus. Nature 406:893-7.
423   3.   Noyce RS, Bondre DG, Ha MN, Lin LT, Sisson G, Tsao MS, Richardson CD. 2011.
424   Tumor cell marker PVRL4 (nectin 4) is an epithelial cell receptor for measles virus.
425   PLoS Pathog 7:e1002240.
426   4.   Muhlebach MD, Mateo M, Sinn PL, Prufer S, Uhlig KM, Leonard VH,
427   Navaratnarajah CK, Frenzke M, Wong XX, Sawatsky B, Ramachandran S, McCray
428   PB, Jr., Cichutek K, von Messling V, Lopez M, Cattaneo R. 2011. Adherens junction
429   protein nectin-4 is the epithelial receptor for measles virus. Nature 480:530-3.
430   5.   Griffin DE, Lin WH, Pan CH. 2012. Measles virus, immune control, and persistence.
431   FEMS microbiology reviews 36:649-62.
432   6.   Rota PA, Moss WJ, Takeda M, de Swart RL, Thompson KM, Goodson JL. 2016.
433   Measles. Nat Rev Dis Primers 2:16049.

434   7.   Kija E, Ndondo A, Spittal G, Hardie DR, Eley B, Wilmshurst JM. 2015. Subacute
435   sclerosing panencephalitis in South African children following the measles outbreak
436   between 2009 and 2011. S Afr Med J 105:713-8.
437   8.   Angius F, Smuts H, Rybkina K, Stelitano D, Eley B, Wilmshurst J, Ferren M, Lalande
438   A, Mathieu C, Moscona A, Horvat B, Hashiguchi T, Porotto M, Hardie D. 2019.
439   Analysis of a Subacute Sclerosing Panencephalitis Genotype B3 Virus from the 2009-
440   2010 South African Measles Epidemic Shows That Hyperfusogenic F Proteins
441   Contribute to Measles Virus Infection in the Brain. J Virol 93:e01700-18.
442   9.   Hardie DR, Albertyn C, Heckmann JM, Smuts HE. 2013. Molecular characterisation
443   of virus in the brains of patients with measles inclusion body encephalitis (MIBE).
444   Virology journal 10:283.
445   10. Mathieu C, Ferren M, Jurgens E, Dumont C, Rybkina K, Harder O, Stelitano D,
446   Madeddu S, Sanna G, Schwartz D, Biswas S, Hardie D, Hashiguchi T, Moscona A,
447   Horvat B, Niewiesk S, Porotto M. 2019. Measles Virus Bearing Measles Inclusion
448   Body Encephalitis-Derived Fusion Protein Is Pathogenic after Infection via the
449   Respiratory Route. J Virol 93:e01862-18.
450   11. Watanabe S, Shirogane Y, Sato Y, Hashiguchi T, Yanagi Y. 2019. New Insights into
451   Measles Virus Brain Infections. Trends Microbiol 27:164-175.
452   12. Mathieu C, Bovier FT, Ferren M, Lieberman NAP, Predella C, Lalande A, Peddu V,
453   Lin MJ, Addetia A, Patel A, Outlaw V, Corneo B, Dorrello NV, Briese T, Hardie D,
454   Horvat B, Moscona A, Greninger AL, Porotto M. 2021. Molecular Features of the
455   Measles Virus Viral Fusion Complex That Favor Infection and Spread in the Brain.
456   mBio doi:10.1128/mBio.00799-21:e0079921.
457   13. Yanagi Y, Ono N, Tatsuo H, Hashimoto K, Minagawa H. 2002. Measles virus
458   receptor SLAM (CD150). Virology 299:155-61.
459   14. Yanagi Y, Takeda M, Ohno S, Hashiguchi T. 2009. Measles virus receptors. Current
460   topics in microbiology and immunology 329:13-30.
461   15. Hashiguchi T, Maenaka K, Yanagi Y. 2011. Measles virus hemagglutinin: structural
462   insights into cell entry and measles vaccine. Frontiers in microbiology 2:247.
463   16. Yin HS, Paterson RG, Wen X, Lamb RA, Jardetzky TS. 2005. Structure of the
464   uncleaved ectodomain of the paramyxovirus (hPIV3) fusion protein. Proc Natl Acad
465   Sci U S A 102:9288-93.
466   17. Lamb RA, Paterson RG, Jardetzky TS. 2006. Paramyxovirus membrane fusion:
467   lessons from the F and HN atomic structures. Virology 344:30-7.
468   18. Yin HS, Wen X, Paterson RG, Lamb RA, Jardetzky TS. 2006. Structure of the
469   parainfluenza virus 5 F protein in its metastable, prefusion conformation. Nature
470   439:38-44.
471   19. Harrison SC. 2008. Viral membrane fusion. Nat Struct Mol Biol 15:690-8.
472   20. Chang A, Dutch RE. 2012. Paramyxovirus fusion and entry: multiple paths to a
473   common end. Viruses 4:613-36.
474   21. Plemper RK, Brindley MA, Iorio RM. 2011. Structural and mechanistic studies of
475   measles virus illuminate paramyxovirus entry. PLoS pathogens 7:e1002058.
476   22. White JM, Delos SE, Brecher M, Schornberg K. 2008. Structures and mechanisms of
477   viral membrane fusion proteins: multiple variations on a common theme. Crit Rev
478   Biochem Mol Biol 43:189-219.
479   23. Sapir A, Avinoam O, Podbilewicz B, Chernomordik LV. 2008. Viral and
480   developmental cell fusion mechanisms: conservation and divergence. Dev Cell 14:11-
481   21.
482   24. Eckert DM, Kim PS. 2001. Design of potent inhibitors of HIV-1 entry from the gp41
483   N-peptide region. Proc Natl Acad Sci U S A 98:11187-92.

25. Porotto M, Carta P, Deng Y, Kellogg GE, Whitt M, Lu M, Mungall BA, Moscona A. 2007. Molecular determinants of antiviral potency of paramyxovirus entry inhibitors. J Virol 81:10567-74.

26. Schmidt AG, Yang PL, Harrison SC. 2010. Peptide inhibitors of flavivirus entry derived from the E protein stem. J Virol 84:12549-54.

27. Vigant F, Lee B. 2011. Hendra and nipah infection: pathology, models and potential therapies. Infectious disorders drug targets 11:315-36.

28. Pessi A, Langella A, Capito E, Ghezzi S, Vicenzi E, Poli G, Ketas T, Mathieu C, Cortese R, Horvat B, Moscona A, Porotto M. 2012. A general strategy to endow natural fusion-protein-derived peptides with potent antiviral activity. PLoS One 7:e36833.

29. Steffen DL, Xu K, Nikolov DB, Broder CC. 2012. Henipavirus mediated membrane fusion, virus entry and targeted therapeutics. Viruses 4:280-309.

30. Miyamoto F, Kodama EN. 2012. Novel HIV-1 fusion inhibition peptides: designing the next generation of drugs. Antiviral chemistry & chemotherapy 22:151-8.

31. Tan JJ, Ma XT, Liu C, Zhang XY, Wang CX. 2012. The Current Status and Challenges in the Development of Fusion Inhibitors as Therapeutics for HIV-1 Infection. Current pharmaceutical design.

32. Lee KK, Pessi A, Gui L, Santoprete A, Talekar A, Moscona A, Porotto M. 2011. Capturing a fusion intermediate of influenza hemagglutinin with a cholesterol-conjugated peptide, a new antiviral strategy for influenza virus. J Biol Chem 286:42141-9.

33. Sato Y, Watanabe S, Fukuda Y, Hashiguchi T, Yanagi Y, Ohno S. 2018. Cell-to-Cell Measles Virus Spread between Human Neurons Is Dependent on Hemagglutinin and Hyperfusogenic Fusion Protein. J Virol 92.

34. Jurgens EM, Mathieu C, Palermo LM, Hardie D, Horvat B, Moscona A, Porotto M. 2015. Measles fusion machinery is dysregulated in neuropathogenic variants. mBio 6.

35. Watanabe S, Shirogane Y, Suzuki SO, Ikegame S, Koga R, Yanagi Y. 2013. Mutant fusion proteins with enhanced fusion activity promote measles virus spread in human neuronal cells and brains of suckling hamsters. Journal of virology 87:2648-59.

36. Hashiguchi T, Fukuda Y, Matsuoka R, Kuroda D, Kubota M, Shirogane Y, Watanabe S, Tsumoto K, Kohda D, Plemper RK, Yanagi Y. 2018. Structures of the prefusion form of measles virus fusion protein in complex with inhibitors. Proc Natl Acad Sci U S A 115:2496-2501.

37. Porotto M, Devito I, Palmer SG, Jurgens EM, Yee JL, Yokoyama CC, Pessi A, Moscona A. 2011. Spring-loaded model revisited: paramyxovirus fusion requires engagement of a receptor binding protein beyond initial triggering of the fusion protein. J Virol 85:12867-80.

38. Figueira TN, Palermo LM, Veiga AS, Huey D, Alabi CA, Santos NC, Welsch JC, Mathieu C, Horvat B, Niewiesk S, Moscona A, Castanho M, Porotto M. 2017. In Vivo Efficacy of Measles Virus Fusion Protein-Derived Peptides Is Modulated by the Properties of Self-Assembly and Membrane Residence. J Virol 91.

39. Porotto M, Yokoyama CC, Orefice G, Kim HS, Aljofan M, Mungall BA, Moscona A. 2009. Kinetic dependence of paramyxovirus entry inhibition. J Virol 83:6947-51.

40. Mathieu C, Huey D, Jurgens E, Welsch JC, DeVito I, Talekar A, Horvat B, Niewiesk S, Moscona A, Porotto M. 2015. Prevention of measles virus infection by intranasal delivery of fusion inhibitor peptides. J Virol 89:1143-55.

41. Welsch JC, Talekar A, Mathieu C, Pessi A, Moscona A, Horvat B, Porotto M. 2013. Fatal measles virus infection prevented by brain-penetrant fusion inhibitors. J Virol 87:13785-94.

534   42.   Mathieu C, Augusto MT, Niewiesk S, Horvat B, Palermo LM, Sanna G, Madeddu S,
535   Huey D, Castanho MA, Porotto M, Santos NC, Moscona A. 2017. Broad spectrum
536   antiviral activity for paramyxoviruses is modulated by biophysical properties of fusion
537   inhibitory peptides. Sci Rep 7:43610.
538   43.   Talekar A, Moscona A, Porotto M. 2013. Measles virus fusion machinery activated by
539   sialic acid binding globular domain. J Virol 87:13619-27.
540   44.   Watanabe S, Ohno S, Shirogane Y, Suzuki SO, Koga R, Yanagi Y. 2015. Measles
541   virus mutants possessing the fusion protein with enhanced fusion activity spread
542   effectively in neuronal cells, but not in other cells, without causing strong
543   cytopathology. J Virol 89:2710-7.
544